

Phototherapy with Gold Nanoparticles and a Diode Laser for Oral Squamous Cell Carcinoma of the Tongue in Rats

Ahmed Abdelatif Abdelaziz¹, Ali Mohamed Saafan², Latifa Mohamed Abdelgawad³, Mahmoud Bawdy El badawy⁴.

¹Oral and maxillofacial surgeon, Ministry of Health, National Bank Hospital, Cairo, Egypt.

²Professor, Department of medical applications of laser, National institute for laser enhanced sciences, Cairo university, Cairo, Egypt.

³Professor, Department of medical applications of laser, National institute for laser enhanced sciences, Cairo university, Cairo, Egypt.

⁴Professor of pathology, Faculty Of veterinary, BaniSwaaf, Egypt.

E-mail: Ahmed.abdelatif.gad@gmail.com¹

Abstract

Photon energy is selectively delivered and transformed into heat sufficient to produce cellular hyperthermia in plasmonic photothermal therapy (PPTT), a minimally invasive oncological therapeutic method. The current study shows that in vivo PPTT treatment of rats is possible. plasmonic gold nanorods and a compact, portable device to treat deep tissue cancers a low-cost near-infrared (NIR) laser. Squamous cell carcinomas shrink dramatically in size in Direct ($P < 0.0001$) and intravenous ($P < 0.0008$) delivery of rats tongue were detected. pegylated gold nanospheres For both administration and tumour growth inhibition Over a 30 day period, resorption of >57 percent of the directly injected techniques was seen, with resorption of >57 percent of the directly injected techniques and a quarter of the intravenously treated tumours.

Keywords: photothermal therapy; nanospheres; hyperthermia; near infrared; polyethylene glycol; nanotechnology.

1. Introduction

Oral squamous cell carcinoma (OSCC) is the sixth most common oral malignancy, with over 500,000 cases diagnosed each year (1). OSCC is thought to be responsible for more than 90% of oral cancer cases and has the highest mortality rate in the world (2-4). OSCC may affect the lips, tongue, upper and lower gingiva, retromolar triangle, alveolar mucosa, mouth floor and palate, buccal mucosa, oropharynx, and salivary glands, among other anatomical structures (2, 7). The lateral boundary of the tongue accounts for 40% of OSCC cases, followed by the floor of the mouth (30%), and the lower lip (10%) (4, 7).

Following the fact that the majority of OSCC cases were the result of prior precancerous lesions, WHO recommended changing the word "precancerous lesions" to "potentially malignant disorders" (PMDs) in 2005. Leukoplakia, erythroplakia, oral lichen planus, oral submucous fibrosis, actinic keratosis, discoid lupus erythematosus, and palatal lesions are some of the PMDs that may occur. When compared to other oral pathologies, these conditions have a significantly higher chance of being cancerous. (3).

Oral cancer is a malignant neoplasm that develops in the mouth. Squamous cells are the histological basis of approximately 90% of oral cancers, so this form of cancer is commonly referred to as OSCC. The OSCC has a low degree of differentiation and a proclivity for lymph node metastasis in the regional lymph nodes. Even though the oral cavity is very accessible during any clinical examination, the majority of OSCC are diagnosed at a very late and crucial point. The key causes in this case are the patient's lack of expertise and, of course,

the doctor's failure to diagnose the disorder properly. Despite the wide range of treatment options, late diagnosis greatly decreases the risk of survival⁽⁴⁾.

The most important risk factors for OSCC, with a prevalence of over 90%, are long-term excessive alcohol intake and tobacco use⁽²⁾. Oral carcinogenesis is a complex mechanism that is influenced by a number of factors. Epithelial cells are affected by genetic mutations during this phase, which ultimately lead to a number of neoplastic sites in the oral cavity; these sites can grow into OSCC over time. If an oral mucosal lesion does not improve after three weeks, it should be treated as a life threatening disease that necessitates biopsy and further histopathological examination⁽⁴⁾.

The traditional oral examination, which involves clinical assessment and palpation of the mucosa of the oral cavity under the illumination of the dental chair, is most commonly used to diagnose a questionable lesion⁽¹⁾. The ability to diagnose OSCC at an early stage is critical in order to lower the high incidence of illness and death among patients⁽⁶⁾. Toluidine blue (TB), Methylene blue staining, Rose Bengal staining, and Lugol's iodine staining are examples of methods. Staining with TB is a well-established method for detecting premalignant and malignant lesions, and it is recommended as part of the clinical evaluation of oral mucosal tissues, especially in high risk patients. These methods are inexpensive, simple to implement, and reliable⁽³⁾. The use of different types of dyes to stain the mucosa in order to identify neoplastic cells, cells with a high reproductive function, and particular areas for analysis and biopsy⁽⁵⁾.

The most prognostic symptom of any malignancy is epithelial dysplasia. Dysplasia is graded as mild, moderate, or extreme by the World Health Organization. These are methods that employ the use of a microscope to assess cells collected from smears, scraping, and needle aspiration through different mucosal depths. The most common findings are a standard mucosal lesion that appears normal at first glance but contains atypical cells when prepared. The cytological tests taken from the oral cavity can aid in identifying and diagnosing tissues with a high risk of cancer⁽⁵⁾.

The most popular treatment methods for oral cancer are noninvasive, such as radiotherapy in most cases, or surgical, such as surgery, which is typically the first treatment choice despite the fact that radiotherapy survival rates and anatomical site control are comparable^(8,9). These techniques may be used individually or in combination. In order to treat the initial tumour, radiotherapy may be given alone or in conjunction with chemotherapy. It can be used as neoadjuvant therapy, which reduces the size of the tumour before surgery. Radiotherapy can also be used as adjuvant therapy, which improves the efficacy of the initial treatment and, as a result, increases the chances of survival, lowers the risk of recurrence, and also improves the symptoms of late-stage oral cancer⁽⁸⁾.

Radiotherapy has a number of significant disadvantages, including xerostomia, osteoradionecrosis, mucositis, and a lengthy treatment time, which are not desirable in situations where the bone is close to the patient and/or the patient is young. Oral cancer treatment techniques such as surgery, radiotherapy, and chemotherapy have a significant impact on the patient's quality of life and are regarded as particularly harsh due to the location and obtrusive nature of the treatment^(7,8). The aim of OSCC treatment methods is to treat the initial tumour while preserving as much shape and function as possible by proper restoration⁽⁹⁾.

The future use of chemically synthesised and functionalized nanoparticles engineered specifically for biomedical applications is the subject of much of the current excitement around nanoscience and nanotechnology. Indeed, nanoparticle-based approaches designed to address the unique diagnostic and therapeutic challenges of cancer can hold the greatest promise for nanochemistry. Although several approaches to nanotechnology-enabled cancer diagnostics and therapeutics are being created, a particularly promising strategy

involves the use of noble metal nanoparticles and light. Metallic nanoparticles, such as gold or silver, have unusually bright colours due to their intense optical resonances⁽¹⁰⁾.

Metal nanoparticles that are illuminated by light sustain surface plasmons, which are coherent oscillations of their valence electrons. The shape and size of the metal nanoparticle nanoparticle, as well as the form of metal and its local atmosphere, all influence the plasmon resonance wavelength⁽¹¹⁾. Nanoparticles with a diameter of less than 100 nm may have high resonant absorption and scattering properties. Metallic nanoparticles' resonant absorption properties result in solid, highly localised photothermal heating when illuminated by lasers, an effect that can be used to trigger cancer cell death and tumour remission. In bioimaging, the light scattering properties can be used to improve contrast. Nanoparticles' inherent properties can be combined to create integrated diagnostic imaging and therapeutics. The optical resonance of nanoshells and spheres, in particular, can be tuned to a wavelength in the near infrared between 700 and 1100 nm, where water absorption is limited and blood and tissue are maximally transmissive⁽¹²⁾.

2. MATERIAL AND METHODS:

▪ Animals and experimental procedure:

The animal experimental protocol used in this study was approved by Institutional Animal Care and Use Committee Cairo university (CU-IACUC CU I F 21 18) , a total of 35 male, 8 weeks old, Wistar rats, body weight (120- 160 g) had been selected for this study . Rats were housed in polypropylene cages (2 rats per cage) each with stainless steel top grill which used for holding pelleted food and filtered drinking water in polycarbonate bottles. The rats were maintained under controlled conditions of temperature (23 ± 2 C), humidity (55 ± 5 %), and a 12:12 h light-dark cycle. Paddy husk was used as bedding material.

▪ Study design.

The animals were randomly divided into four groups:

Group (A): composed of 5 rats (control negative without tumor induction) as a baseline control group. One animal was euthanized at day zero and four were euthanized at end of the experiment.

Group (B): composed of 5 rats (control positive without any treatments after Tumor induction). Animals were painted three times per week, on the tongue surface, with the carcinogen (DMBA) for 12 weeks then followed up for another 4 weeks. A camel hairbrush, number 4, was used for painting⁽²⁰⁾.

Group (C): composed of 12 rats had been injected with 1.5mg/kg body weight of gold nanoparticles in phosphate buffer solution into the tail vein⁽²¹⁾.

Group (D): composed of 13 rats had been injected with 1.5mg/kg body weight of gold nanoparticles in phosphate buffer solution into the tongue tumors under general anesthesia with Ketalar 10 mg/ml (Pfizer AS, Lysaker, Norway) and Zoletil (0.25 mg/kg; Virac Lab, Carros, France) had been irradiated by low level laser therapy irradiation.^(13,14)

▪ Oral tumors

had been developed in the tongue of rats using topical application of the carcinogen 0.5% 7,12-dimethylbenz (a) anthracene (DMBA) dissolved in heavy mineral oil (U.S.P), Chlorauric acid, Poly [ethylene glycol], Thymoquinone, Folic acid and Phosphate-buffered saline (PBS), PH=7.4. All the previous chemicals were from Sigma-Aldrich Company, Saint Louiss, USA (three times a week for 12 weeks)^(15,16,17,20).

Diode laser

In this analysis, gallium-aluminum-arsenide (GaAlAs) diode laser equipment was used to provide a continuous 808 nm wavelength and (808 nm, 6 mm dia) and it was determined that 10–15 minutes of irradiation at 0.9W/cm² was necessary for maximal tumor control and minimal damage to surrounding tissues. The tongue tumor was in no contact with the probe.

LLLT was administered three times per week to the day of euthanasia, after 24 h post-AuNP injection⁽¹⁸⁾.

Synthesis and Characterization AuNPs .

100 mL of 0.01 percent chloroauric acid ($\text{HAuCl}_4 \cdot 4\text{H}_2\text{O}$) solution and 5 mL of clove bud aqueous extract were used to synthesize the AuNP. Using the dilute NaOH buffer solution, the pH value of the biologically functionalized gold nanoparticle solution was changed to 7.4, equivalent to the physiological condition of the rats. In order to eliminate the precipitates, aggregates, fibrous matter and other unreacted water soluble impurities, the AuNP solution was filtered through 1 μm filters and the filtrate was stored at 4 °C in order to avoid aggregation.

The gold suspension nanoparticle (1 mL) was centrifuged for 30 minutes at 10,000 rpm and the supernatant was removed. The size and shape of the gold nanoparticles were examined using an FEI Nova nano 600, Netherlands field emission scanning electron microscopy and the images worked at 15 kV at a 0 tilt position⁽¹⁹⁾. A transmission electron microscopy using a Hitachi HF-2000 field emission high-resolution transmission electron microscopy operating at 200 kV was used to examine the size and morphology of the gold nanoparticles. The optical absorption spectra in the wavelength range of 200-850 nm were measured in a 5 mL glass cuvette using a DU800 spectrometer.

Parameters evaluated

1. Clinical observation

Both animals with symptoms of toxicity (morbidity) were observed twice a day. & Mortality). There has been a detailed clinical examination It's once a week. Animals during the comprehensive clinical exam Their cages were removed and inspected for skin, hair, eyes, Tremors, convulsions, gait and stance, salivation, pilot erection, Production etc⁽²²⁻²⁴⁾.

2. Ophthalmic examination

Prior to care and during the week, eyes were examined Using an ophthalmoscope prior to sacrifice after inducing the Mydriatic agent, Tropicamide at 1 percent. The cornea, lens, iris, retina, vitreous, humour and optic disc nerve were present during the examination⁽²²⁻²⁴⁾.

3. Body weight and food consumption

Prior to surgery, the body weights of all animals were assessed and on days 8, 15, 22 and 29, respectively. Fasting weight on the body was reported on Day 30 prior to the sacrifice. Consumption of food was assessed once a week and the average daily intake of food per week the animal was measured for each weighing cycle⁽²²⁻²⁴⁾.

4. Hematology and blood chemistry

On treatment day 29, animals were fasted overnight, and blood fasted. Samples were collected on the 30th day by retro-orbital puncture from all rodents. Blood samples were taken from the dipotassium EDTA collection. Tubes as hematological anticoagulants and without anticoagulants The Clinical Chemistry Tubes. Hematological parameters such as nitrogen urea (BUN), creatinine (CRE), creatine kinase, amino transferase aspartate (AST), Using the ARTOS Vesatis biochemical analyser, alanine amino transferase (ALT), cglutamyltranspeptidase (c-GT) and alkaline phosphatase (ALP) were assessed⁽²²⁻²⁴⁾.

5. Urinalysis

On day 29, urine samples from rats were obtained by putting them in individual metabolic cages after fasting overnight. They measured parameters such as pH, glucose, bilirubin, ketone, protein, urobilinogen, nitrite, specific gravity, erythrocytes, and leukocytes⁽²²⁻²⁴⁾.

6. Necropsy and gross examination

Necropsia was performed in all rats on day 30 after the blood collection and was subjected to a thorough macroscopic examination. All rats were sacrificed, measured, exsanguinated and subjected to thorough necropsy by anaesthetic with isoflurane⁽²²⁻²⁴⁾.

7. Histopathology

For histopathological tests, the following organs and tissues were collected: tongue, liver. In Davidson's fixative, the tissues were fixed in 10 percent neutral buffered formalin and Microscopic examinations were carried out for all control slides. In short, hematoxyline and eosin (H & E) were stained with 4-5 mm microtome sections following a standard staining protocol for histopathological staining⁽²²⁻²⁴⁾.

8. BCL-2 Immunohistochemistry

Even when tumours have the same clinical and histopathological characteristics, these parameters of aggressive tumour activity may differ. As a result, in order to better determine tumour natural history and, at the same time, to look for molecular markers that could predict outcomes by analysing clinical data.

3. Statistical analysis

The data was statistically analyzed and reported as mean \pm SD. Bartlett's test for homogeneity of variance was used to analyze the data for mean body weight, food consumption, hematology, clinical chemistry and organ weight. On homogeneous data, oneway variance analysis (ANOVA) was performed. For multiple comparisons, Dunnett's test was used.

3. Results and Discussion

The size and shape of the gold nanoparticles were well defined and uniform in shape, with a normal distribution, according to transmission electron microscopy (TEM) images. The size of the particles was 50 nm, and their morphology was spherical, as shown in **Figure 1 A**.

Clinical findings: In comparison to the control group, animals painted with DMBA displayed hair loss, significant weight loss, red macules and papules and tongue ulcers. Papillary overgrowth were discovered intra and perioral, and they increased in size by the end of the study. By the 16th week, gold nanoparticles only had been administered to the animals (group C). When compared to group D, animals treated with gold nanoparticles with laser showed significant weight gain and a reduction in papillary overgrowth size, leading to complete ablation of ulcers and small tumors more than (group C) **Figure 2**.

Histopathologic results (Figure 3):

- The mucosa in Group A (the negative control) was regular, with four distinct layers.
- Group B (DMBA group) had well to moderately differentiated oral squamous cell carcinoma (OSCC) with various ulcers and significant papillomatous overgrowths, as well as several invading malignant epithelial islands into the connective tissue. The epithelium as a whole displayed hyperplasia and hyperkeratinization, as well as dysplasia.
- Group C (gold nanoparticles) Congestion and mononuclear infiltration and Sub epithelial mild congestion and inflammatory cell infiltration.
- Group D (gold nanoparticles with laser) normal tongue (epidermis, muscle)

Apoptotic cells were discovered as smaller cells with nuclear fragmentation, cytoplasm condensation, and cell borders that were clearly defined. **Figure 1**

D: TEM images Presence of gold nanoparticles in the tongue tissue.

Results of blood analysis:

The effects of 50 nm GNPs on the blood serum of rats were assessed using biochemical parameters such as AST, GGT, ALT, ALP, UREA, and CREA. The administration of gold nanoparticles (135 ± 43.53 ; Mean SE) and gold nanoparticles with laser (139 ± 21.02) 50 nm GNPs increased the AST values in this study as compared to the control (130 ± 23.26). the AST values increased significantly⁽²⁵⁾. This research suggests that GNP administration can cause minor liver damage, and that GNPs have a direct effect on liver function. Serum is a form of liquid that is used AST and ALT levels are typical markers for hepatic toxicity: when the liver is impaired by some cause, such as hepatitis or cirrhosis, the levels of these proteins

rise rapidly **Figure 1:-** TEM images show **B:** Presence of gold nanoparticles in the cytoplasm of liver cells from rats sacrificed after 29 days from the local injection of AuNPs. **C:** Presence of gold nanoparticles in phagolysosomes in Kupffer cells of the liver ⁽²⁵⁾.

Hepatocyte swelling could be caused by membrane dysfunction, which results in a large influx of water and Na⁺ due to GNP effects, as well as leakage of lysosomal hydrolytic enzymes, which causes cytoplasmic degeneration and macromolecular crowding. ⁽²⁶⁻³²⁾ the vacuolated swelling of the cytoplasm of the GNP-treated rats' hepatocytes could indicate GNP-induced acute and subacute liver injury. These changes were size-dependent, with smaller ones causing the most effects, and they were linked to GNP exposure time ⁽²⁶⁻³²⁾. After intraperitoneal administration of 13 nm colloidal gold beads, the largest volume of gold was found in the liver and spleen ⁽³³⁾. In another analysis, gold nanorods (65± 5 nm) were injected intravenously and found to accumulate primarily in the liver within minutes. ⁽³⁴⁾ **(Fig. 4).**

The GGT values increased with the administration of gold nanoparticles (25± 1.36; Mean & SE) and gold nanoparticles with laser (22 ± 1.36; Mean & SE) nm GNPs compared to the control (15± 1.74). When 50 nm GNPs were used instead of the GGT values were significantly (Fig. 5). the ALT values decreased in gold nanoparticles (40.5± 6.01; Mean & SE) and gold nanoparticles with laser (39 ± 7.32) nm GNPs were administered for a 29-day exposure period, compared to the control (44± 10.09). When 50 nm GNPs were used instead of power, the ALT values dropped dramatically (Fig. 6). The ALP values significantly decreased in gold nanoparticles (196.60± 33.95; Mean & SE) and gold nanoparticles with laser (251.60± 38.52) nm GNPs were administered, as compared to the control (347± 52.52) (Fig. 7). The levels of CREA values increased in gold nanoparticles (0.85± 0.02; Mean & SE) and gold nanoparticles with laser (0.74± 0.05) nm GNPs were administered, in a non significant manner relative to the control (0.6± 0.06) (Fig 8).

The UREA values increased when gold nanoparticles (43.56± 1.68; Mean SE) and gold nanoparticles with laser (44.18± 2.59) were administered, in a non-significant manner relative to the control (38.36± 3.36) group (Fig. 9). The non-significant increases in UREA and CREA levels may be due to the highest GNP clearance through the kidney. After regular injections of GNPs, the amount of gold in the kidney increased significantly. Surprisingly, as the GNP dose rises, the percent gold accumulated decreases, implying that GNPs are efficiently cleared from the body (35). UREA, CREA, total bilirubin, and ALP levels in rats' blood serum were measured to assess kidney, hepatic, and biliary function. When all of these metabolites in the serum of animals treated with different doses of GNPs were compared to controls, no statistically significant differences in any of the parameters tested were found ⁽³⁵⁾. After GNP is absorbed via inhalation, oral, or dermal exposure, it is distributed across the body through the bloodstream. The size and exposure time of the injected particles had an effect on the distribution of GNPs. At 29 days after injection, the smallest GNPs showed the most widespread tissue distribution ⁽²⁸⁻³²⁾. Cloudy swelling, vacuolar degeneration, hyaline droplets and casts were all observed after exposure to GNP doses. There was mild congestion in the glomeruli, but no hypercellularity or basement membrane thickening. The cortex and proximal renal convoluted tubules were more affected than the distal tubules. Cloudy swelling, renal tubular necrosis, intertubular blood capillary dilation and inflammatory cell infiltrations were also found ⁽²⁸⁻³²⁾.

BCL-2 Immunohistochemistry

The disease's progression in each patient. Signaling molecules involved in the regulation of proliferation and cell death, specifically genes of the bcl-2 family, have received a lot of attention in both normal and neoplastic tissue ⁽³⁶⁾. Apoptosis is a genetically controlled process that is essential for normal tissue homeostasis as well as neoplastic transformation ⁽³⁷⁾. The bcl-2 family of apoptosis-related genes is divided into two groups: proapoptotic genes like bax, evil, and bcl-xs, and antiapoptotic genes like bcl-2, bcl-xL, and mcl-

1⁽³⁸⁾. These genes' protein products may both homo- and heterodimerize, and the proportion between the two classes can cause the cell to join apoptotic or proliferative programmes to divide in an unregulated manner⁽³⁹⁾.

When the bcl-2 genes are activated, their proteins are normally overexpressed. Bcl-2 is one of the most studied antiapoptotic proteins. Its abnormal expression has been identified in a variety of solid tumours, including lung cancer, thyroid cancer, breast cancer, ovarian cancer, stomach cancer, and colon cancer^(40,41). The bcl-2 protein protects cells from death by slowing or preventing apoptosis, as well as promoting tumour growth⁽⁴²⁾. Because of its ability to suppress chemo/radiotherapy-induced apoptosis, overexpression of bcl-2 has been linked to a poor response to therapy in many tumours⁽⁴³⁾. There was a potential connection between the normal prognostic parameters and the expression of bcl-2, as well as to evaluate the apoptosis can play a role in the pathogenesis of OSCCs. In our work the level of bcl-2 in group C more than group D which indicated that the effect of treatment of gold nanoparticless combined with laser more effect than gold nanoparticless only for treatment of squamous cell carcinoma of tongue.

Initially, 13 rats from Group D were used to determine the best circumstances for near-infrared PPTT treatment of an SCC tumour on the tongue of rats. 15 µl of pegylated gold spheres were injected directly into the tumour interstitium, and 100 µl were infused intravenously (tail). Tumours directly injected with nanospheres were exposed to extracorporeal NIR (808 nm, 6 mm dia) after 24 hours, and it was shown that 10–15 minutes of irradiation at 0.9 W/cm² was required for optimal tumour control and minimal tissue damage (group D).

Furthermore, compared to intravenous nanosphere injections, direct injection of pegylated gold nanospheres with near-infrared PPTT inhibited tumour resorption and growth. Changes in tumour volume were measured over a 29-day period for control rats, as well as those treated with intravenous and direct nanosphere injections followed by PPTT (Fig. 10), and statistical hypothesis testing for differences in average tumour growth was performed using previously established treatment conditions (Table 2). At day 29, (Figure 10) indicates a >96% decrease in average tumour growth for SCC that was treated directly and a >74% decrease in average tumour growth for SCC that was treated intravenously (Relative to control tumors). The average tumour growth for directly and intravenously treated tumours at day 29 was considerably lower than the untreated control groups (P0.0001 and P0.0008, respectively). During the experiment, differences in observed efficacy for direct and intravenous treatments gradually developed, reaching statistical significance on day 29. At the end of the experiment, non-parametric analysis of variance revealed statistically significant differences between the treated and untreated groups (Table 3). The selectivity and specificity of near-infrared PPTT are clearly demonstrated by these findings.

Selective hyperemia of malignant tissues treated with pegylated gold nanorods by near-infrared PPTT is related to the substantial changes in observed SCC tumour development. The EPR effect causes a preferential concentration of pegylated gold nanorods within the tumour interstitium⁽⁴⁴⁾. Tumour cells are increasingly vulnerable to hyperthermic effects^(45, 46) such as disruption of metabolic signalling processes, protein denaturation, and the onset of acidosis or apoptosis caused by the production of heat-shock proteins and other immune stimulants due to their rapid metabolic rates. Nuclea are known to be disrupted by small increases in local temperature⁽⁴⁸⁾. Hyperthermic injury can cause compromised vascular supply and endothelial edema in extreme cases⁽⁴⁵⁾, and microthrombosis in the context of homeostasis⁽⁴⁷⁾. Mild hyperthermia has been demonstrated to inhibit cell surface receptor activity, membrane transport, and RNA and DNA polymerization during protein synthesis in vitro. Hyperthermia has also been demonstrated to impair DNA polymerase and mediated repair of sublethal cell damage, such as that sustained during radiotherapy. While tumour

growth inhibition and resorption are most likely the consequence of a combination of the aforementioned effects, it is assumed that ablation of the tumour vasculature and localised membrane rupture is the most important. Hyperthermia has also been demonstrated to impair DNA-polymerase and mediated repair of sublethal cell damage, such as that sustained during radiotherapy. While tumour growth inhibition and resorption are most likely the consequence of a combination of the aforementioned effects, it is assumed that ablation of the tumour vasculature and localised membrane rupture is the most important.

Although the mechanism of cellular response in the present example is yet to be elucidated, the specificity of hyperthermic effects on tumour growth from direct nearinfrared PPTT treatments is apparent ($P < 0.0001$, respectively). InhibitionThe local technique shows average tumour growth with minimal harm to adjacent tissues. In pre-clinical conditions, resorption of $>57\%$ of directly injected tumours and 25% of intravenously treated tumours clearly suggests the potential curative and adjunctive applications of NIR plasmonic photothermal treatment (PPTT). This research indicates that in the future, synthesis and metabolism of various GNP, as well as liver safety, would be more important issues for medical applications of gold based nanomaterials. As a result, further kinetic and toxicokinetic studies are needed to expand our understanding of particle activity in vivo.

4. Conclusion

Photodynamic therapy is a promising therapeutic alternative in the treatment of cancer. However, because to the drawbacks of traditional PSs, it has yet to acquire acceptability as a first line therapy choice. The use of nanoparticles in PDT, particularly gold nanoparticles, is a very promising strategy for future technical breakthroughs, and gold nanoparticles have a lot of potential for tumour therapy. There are still certain limits in clinical use for PPT, PDT, and drug delivery functions in cancer treatment. To begin, the number of nanoparticles accumulating in tumours must be accurately measured. Quantification approaches must be used with conventional illumination geometries of malignancies in specific organs in order to totally destroy cancers.

Currently, the majority of in vivo studies have been conducted on subcutaneous cancer disorders using NIR light that penetrates a few inches through the skin surface. Fiber optic probes should be used to provide NIR light to deep cancer tissue therapeutics, and particular imaging modalities should be integrated to monitor treatment. Compared to previous gold nanoparticle based phototherapies, gold nanoparticle-assisted radiation therapy can cure cancers deep into the body; nevertheless, recent papers have produced conflicting results on the effects of photon energy and GNP size. In conclusion, due to its excellent selectivity and low side effects, GNP-based cancer treatment has gained a lot of attention in recent years. In vitro and in vivo, gold nanoparticles have shown significant promise as a light-to-heat converter, local field enhancement, medication carrier, and radiation sensitizer for cancer treatment, efficiently damaging malignant tumours. Furthermore, significant progress has been achieved in generating GNP-mediated multifunctional nanoparticles systems, suggesting that a combination therapy method for improving cancer therapeutic efficiency could be introduced in the near future. However, important obstacles must be overcome before these technologies can be implemented in clinics, such as GNP nonbiodegradability and limited light penetration depth. As a result, more research is needed to improve the nanostructure's in vivo behaviour, and the long-term effects of GNPs lingering in organs like the liver and spleen should be better known. Overall, as research and technology advance, GNP-mediated therapies are more likely to be adopted for cancer clinical treatment with a less invasive nature.

5. Acknowledgments

The author would like to thank Professors **Ali Mohamed Saafan, Latifa Mohamed Abdelgawad and Mahmoud Bawdy El badawy** for their information and helpful discussions.

6. Conflict of interest

No conflict of interest declared.

7. References

1. Giovannacci, I., Vescovi, P., Manfredi, M. and Meleti, M. (2016). Non-invasive visual tools for diagnosis of oral cancer and dysplasia: A systematic review. *Medicia Oral y CirugiaBucal*, pp.e305-e315.
2. Maleki, D., Ghojzadeh, M., Mahmoudi, S., Mahmoudi, S., Pournaghi-Azar, F., Torab, A., Piri, R., Azami-Aghdash, S. and Naghavi-Behzad, M. (2015). Epidemiology of Oral Cancer in Iran: a Systematic Review. *Asian Pacific Journal of Cancer Prevention*, 16(13), pp.5427-5432.
3. Liu, D., Zhao, X., Zeng, X., Dan, H. and Chen, Q. (2016). Non-Invasive Techniques for Detection and Diagnosis of Oral Potentially Malignant Disorders. *The Tohoku Journal of Experimental Medicine*, 238(2), pp.165-177.
4. Essentials of oral cancer. (2015). *International Journal of Clinical and Experimental Physiology*, 8 (9), pp.11884-11894.
5. Carreras-Torras, C. and Gay-Escoda, C. (2015). Techniques for early diagnosis of oral squamous cell carcinoma: Systematic review. *Medicina Oral Patologıa Oral y CirugiaBucal*, pp.e305-e315.
6. Mascitti, M., Orsini, G., Tosco, V., Monterubbianesi, R., Balercia, A., Putignano, A., Procaccini, M. and Santarelli, A. (2018). An Overview on Current Non-invasive Diagnostic Devices in Oral Oncology. *Frontiers in Physiology*, 9.
7. Pałasz, P., Adamski, Ł., Górska-Chrzastek, M., Starzyńska, A. and Studniarek, M. (2017). Contemporary Diagnostic Imaging of Oral Squamous Cell Carcinoma – A Review of Literature. *Polish Journal of Radiology*, 82, pp.193-202.
8. Ketabat, F., Pundir, M., Mohabatpour, F., Lobanova, L. and Koutsopoulos, S. (2019). Controlled Drug Delivery Systems for Oral Cancer Treatment—Current Status and Future Perspectives. *Pharmaceutics*, 11(7), p.302.
9. Arya, S., Rane, P. and Deshmukh, A. (2014). Oral cavity squamous cell carcinoma: Role of pretreatment imaging and its influence on management. *Clinical Radiology*, 69(9), pp.916-930.
10. Bohren, C. F.; Huffman, D. R. *Absorption and Scattering of Light by Small Particles*; John Wiley and Sons, Inc: New York, 1983.
11. Halas, N. J. Playing with Plasmons: Tuning the Optical Resonant Properties of Nanoshells. *MRS Bull.* 2005, 30, 362–367.
12. Weissleder, R. A Clearer Vision for in Vivo Imaging. *Nat. Biotechnol.* 2001, 19, 316– 317.
Hainfeld J, Dilmanian F, Zhong Z: Gold nanoparticles enhance the radiation therapy of a murine squamous cell carcinoma. *Phys Med Biol.* 2010; 55:3045–59.
14. Ma M, Chen H, Chen Y: Au capped magnetic core/ mesoporous silica shell nanoparticles for combined photothermo-/chemo-therapy and multimodal imaging. *Biomaterials.* 2012; 33:989- 98.
15. Asokan M, Rajamanickam B, Shanmugam M: Emodin down regulates cell proliferation markers during DMBA induced oral carcinogenesis in golden Syrian hamsters. *Manoharan Afr J Tradit Complement Altern Med.* 2016; 14:83-91.
16. Chen X, Duan N, Zhang C: Survivin and tumorigenesis: molecular mechanisms and therapeutic strategies. *J Cancer.* 2016 7:314– 23

17. Li N, Chen X, Liao J: Inhibition of 7, 12 dimethylbenz[a]anthracene (DMBA)-induced oral carcinogenesis in hamsters by tea and curcumin. *Carcinogenesis*.2002; 23:1307-13.
18. SURBHI L, SUSAN E, CLARE, NAOMI J. HALAS: Nanoshell-Enabled Photothermal Cancer Therapy: Impending Clinical Impact. *acco chemic resear*.2008 ;41: 1842-51.
19. Turkevich J, Stevenson PC, Hillier J. A study of the nucleation and growth processes in the synthesis of colloidal gold. *Discuss Faraday Soc*. 1951;11:55–75.
20. Shklar G. The effect of manipulation and incision on experimental carcinoma of hamster buccal pouch.*Cancer Res*. 1968; 28:2180-2182.
21. Huang X, Jain PK, El-Sayed IH, El-Sayed MA. Plasmonic photothermal therapy (PPTT) using gold nanoparticles. *Lasers Med Sci*. 2008; 23:217-228.
22. Zhang XD, Wu D, Shen X, Liu PX, Fan FY, Fan SJ. In vivo renal clearance, biodistribution, toxicity of gold nanoclusters.*Biomaterials*. 2012;33:4628-38.
23. Sung JH, Ji JH, Park JD, Song MY, Song KS, Ryu HR, et al. Subchronic inhalation toxicity of gold nanoparticles. *Part Fibre Toxicol*. 2011;8:16.
24. Zhang XD, Wu HY, Wu D, Wang YY, Chang JH, Zhai ZB, et al. Toxicologic effects of gold nanoparticles in vivo by different administration routes. *Int J Nanomed*. 2010;5:771-81.
25. De Jong, Wim H., Hagens, Werner I., Krystek, Petra, Burger, Marina C., Slips, Adrie " nne J.A.M., Geertsma, Robert E., 2008. Particle size-dependent organ distribution of gold nanoparticles after intravenous administration. *Biomaterials* 29, 1912–1919.
26. Sheth, S.G., Flamm, S.L., Gordon, F.D., Chopra, S., 1998. AST/ ALT ratio predicts cirrhosis in patients with chronic hepatitis C virus infection. *The American Journal of Gastroenterology* 93, 44–48.
27. Abdelhalim, M.A.K., 2012a. Exposure to gold nanoparticles produces pneumonia, fibrosis, chronic inflammatory cell infiltrates, congested and dilated blood vessels, and hemosiderin granule and emphysema foci. *Journal of Cancer Science & Therapy* 4 (3), 046– 050.
28. Abdelhalim, M.A.K., Jarrar, B.M., 2011a. Gold nanoparticles administration induced prominent inflammatory, central vein intima disruption, fatty change and Kupffer cells hyperplasia. *Lipids in Health and Disease* 10, 133.
29. Abdelhalim, M.A.K., Jarrar, B.M., 2011b. Gold nanoparticles induced cloudy swelling to hydropic degeneration, cytoplasmic hyaline vacuolation, polymorphism, binucleation, karyopyknosis, karyolysis, karyorrhexis and necrosis in the liver. *Lipids in Health and Disease* 10, 166.
30. Abdelhalim, M.A.K., Jarrar, B.M., 2011c. Renal tissue alterations were size-dependent with smaller ones induced more effects and related with time exposure of gold nanoparticles. *Lipids in Health and Disease* 10, 163.
31. Abdelhalim, M.A.K., Jarrar, B.M., 2011d. The appearance of renal cells cytoplasmic degeneration and nuclear destruction might be an indication of GNPs toxicity. *Lipids in Health and Disease* 10, 147.
32. Abdelhalim, M.A.K., 2011a. Exposure to gold nanoparticles produces cardiac tissue damage that depends on the size and duration of exposure. *Lipids in Health and Disease* 10, 205.
33. Hillyer, J.F., Albrecht, R.M., 1999. Correlative instrumental neutron activation analysis, light microscopy, transmission electron microscopy, and X-ray microanalysis for qualitative and quantitative detection of colloidal gold spheres in biological specimens. *Microscopy and Microanalysis* 4, 481–490.
34. Niidome, T., Yamagata, M., Okamoto, Y., Akiyama, Y., Takahishi, H., Kawano, T., et al, 2006. PEG-modified gold nanorods with a stealth character for in vivo application. *Journal of Control Release* 114, 343–347.
35. Lasagna-Reeves, C., Gonzalez-Romero, D., Barria, M.A., Olmedo, I., Clos, A., Ramanujam, V.M.S.A., Urayama, A., Vergara, L., Kogan, M.J., Soto, C., 2010. Bioaccumulation and

- toxicity of gold nanoparticles after repeated administration in mice. *Biochemical and Biophysical Research Communications* 393, 649–655.
36. REED, J.C. et al. 1994. Bcl-2 and the regulation of programmed cell death. *J Cell.Biol.* 124: 1–6.
 37. KERR, J.F., C.M. WINTERFORD & B.V. HARMON.1994. Apoptosis: its significance in cancer and cancer therapy. *Cancer* 73: 2013–2026.
 38. BOISE, L.H. et al. 1995. Bcl-2 and Bcl-2 related proteins in apoptosis regulation. *Curr.Top.Microbial.Immunol.* 200: 107–121.
 39. OLTVAI, Z.N., C.L.MILLIMAN & S.J. KORSMEYER. 1993. Bcl-2 heterodimerizes in vivo with a conserved homolog, Bax, that accelerates programmed cell death. *Cell* 74: 609–619.
 40. BINDER, C. et al. 1997. Differential expression of apoptosis associated genes bax and bcl-2 in ovarian cancer. *Anticancer Res.* 17: 2233–2240.
 41. PEZZELLA, F. et al. 1993. Bcl-2 protein in non-small lung carcinoma. *N. Engl. J.Med.* 329: 690–694.
 42. BIRCHALL, M.A. et al. 1997. Apoptosis, mitosis, PCNA and bcl-2 in normal, leukoplakic and malignant epithelia of the human oral cavity. *Oral Oncol.* 33: 419–425.
 43. WAGNER, C. et al. 1996. Induction of death-promoting gene bax-alpha sensitizes cultured breast cancer cells to drug-induced apoptosis. *Int J. Cancer* 67: 138–141.
 44. Maeda H. The enhanced permeability and retention (EPR) effect in tumor vasculature: The key role of tumor-selective macromolecular drug targeting. *Adv Enzyme Regul.* 2001; 41:189–207. [PubMed: 11384745]
 45. Hildebrandt B, Wust P, Ahlers O, Dieing A, Sreenivasa G, Kerner T, Felix R, Riess H. The cellular and molecular basis of hyperthermia. *Critical Reviews in Oncology Hematology.* 2002; 43:33–56.
 46. Huff TB, Tong L, Zhao Y, Hansen MN, Cheng JX, Wei A. Hyperthermic effects of gold nanorod on tumor cells. *Nanomedicine.* 2007; 2:125–132. [PubMed: 17716198] and molecular basis of hyperthermia. *Critical Reviews in Oncology Hematology.* 2002; 43:33–56.
 47. Kowal-Vern A, McGill V, Walenga JM, Gamelli RL. Antithrombin III concentrate in the acute phase of thermal injury. *Burns.* 2000; 26:97–101. [PubMed: 10630326]
 48. Li GC, Mivechi NF, Weitzel G. Heat-Shock Proteins, Thermotolerance, and Their Relevance to Clinical Hyperthermia. *Int J Hyperthermia.* 1995; 11:459–488. [PubMed: 7594802].

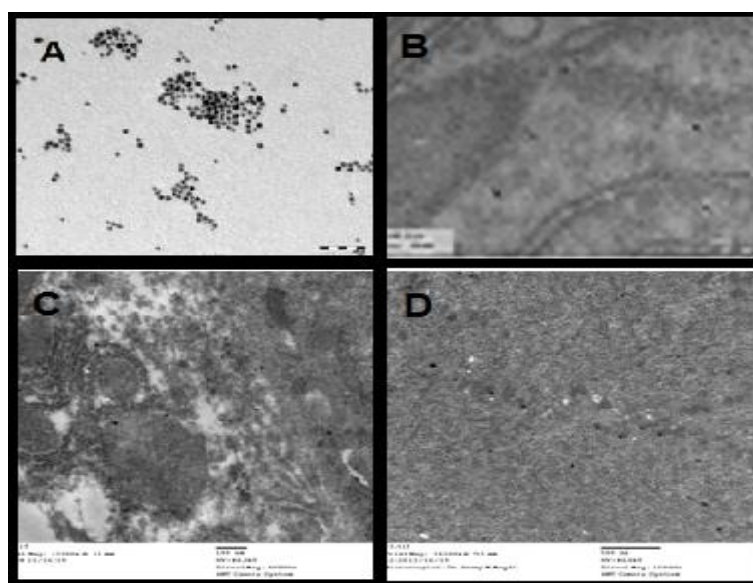


Figure 1: TEM images **A:** size distribution of gold nanoparticles, **B:** Presence of gold nanoparticles in the cytoplasm of liver cells from rats sacrificed after 29 days from the local

injection of AuNPs. **C:** Presence of gold nanoparticles in phagolysosomes in Kupffer cells of the liver. **D:** Presence of gold nanoparticles in the tongue tissue.

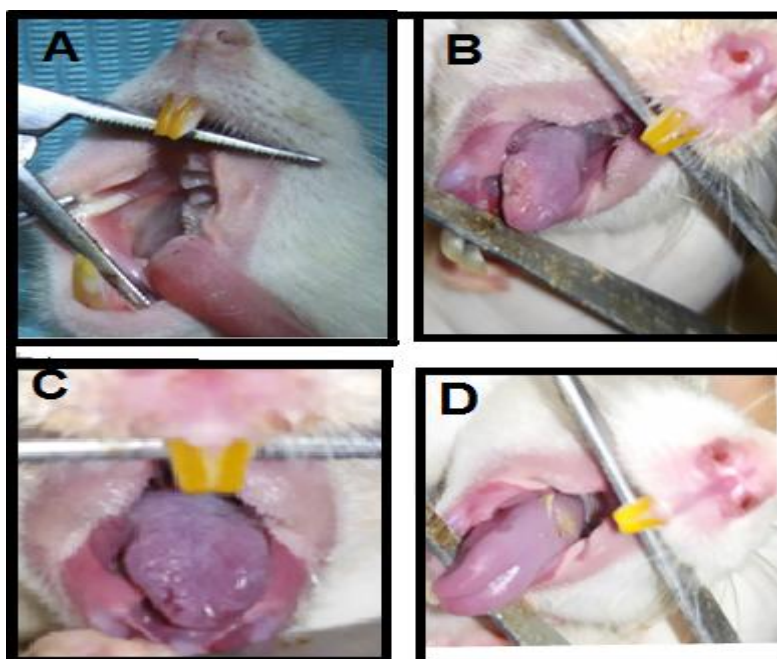


Figure 2: Clinical images show all groups (**A:** negative control group), (**B:** positive control at 16 weeks, (**C:** nanogold group after treatment) where a significant decrease in ulcers and tumor volume, gold (**D:** nanoparticles with-laser) note the overall reduction of ulcers and tumor volume in groups injected with AuNPs accompanied with laser induced the highest recorded ulcer and tumor reduction rate.

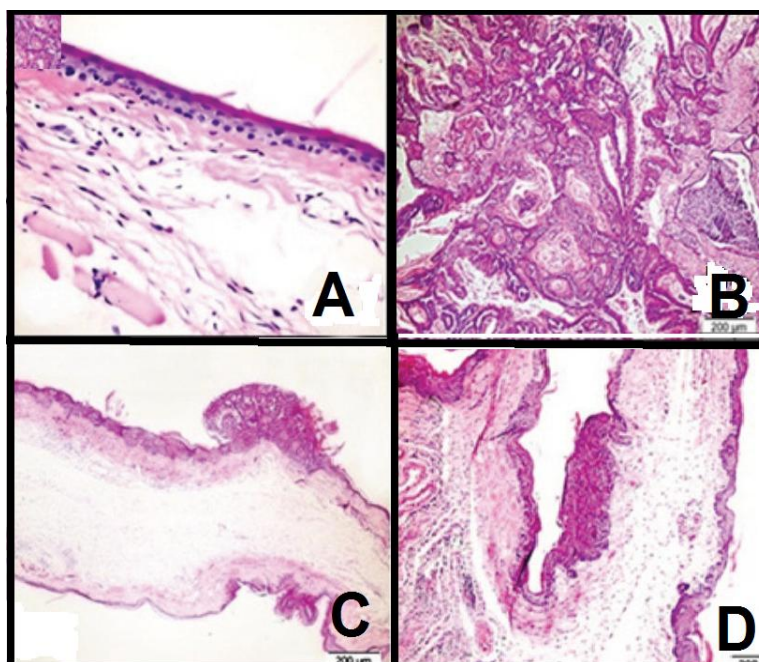


Figure 3: A combined picture representing histopathologic sections, of all groups at end of the 16th week. **A:** untreated group (H&E, x20), **B:** control positive group, **C:** gold

nanoparticles group, **D**: gold nanoparticles with laser laser group, group (from B-D: H&E x4).

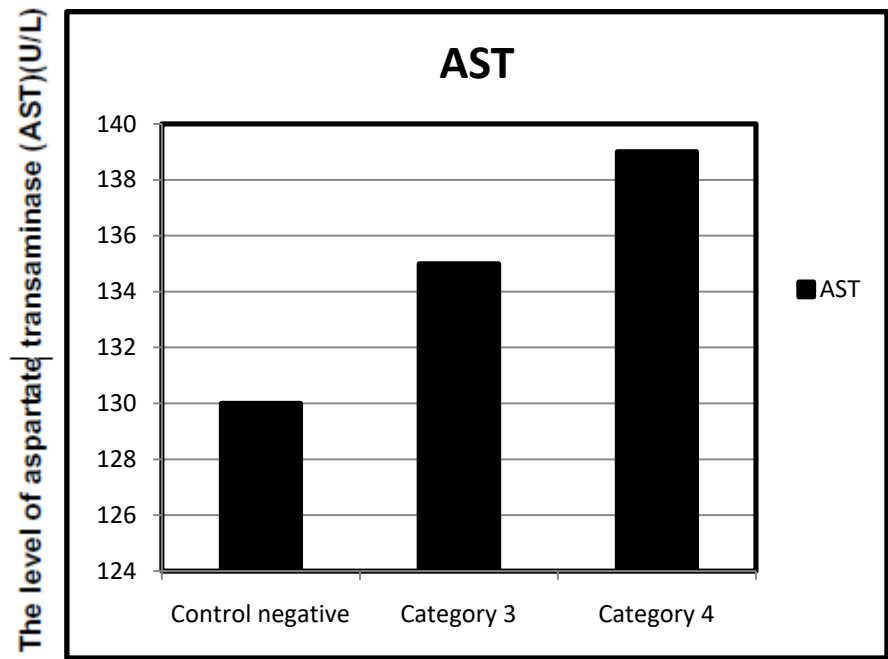


Figure 4: The levels of aspartate transaminase (AST) in different groups’ blood serum.

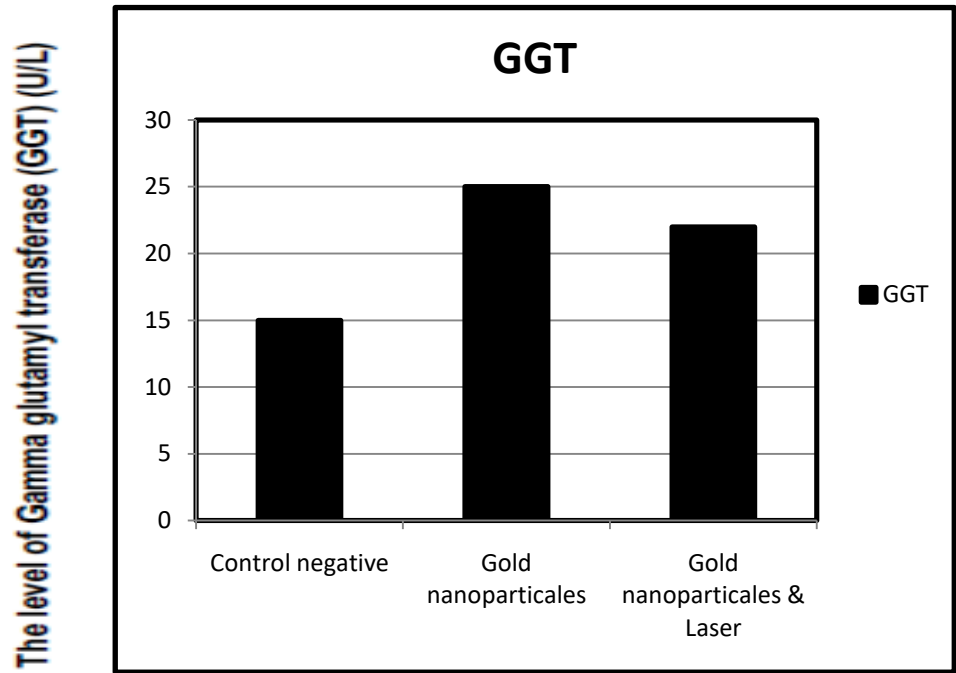


Figure 5: The levels of gamma glutamyltransferase (GGT) in different groups’ blood serum.

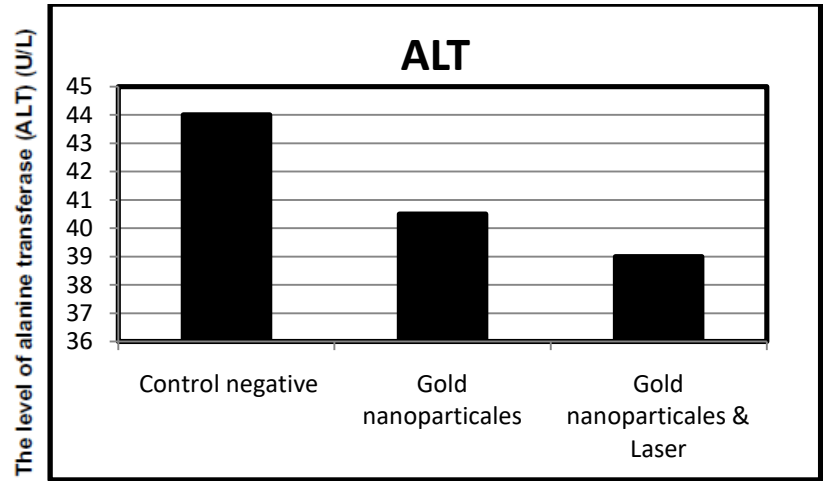


Figure 6: The levels of alanine transferase (ALT) in different groups’ blood serum.

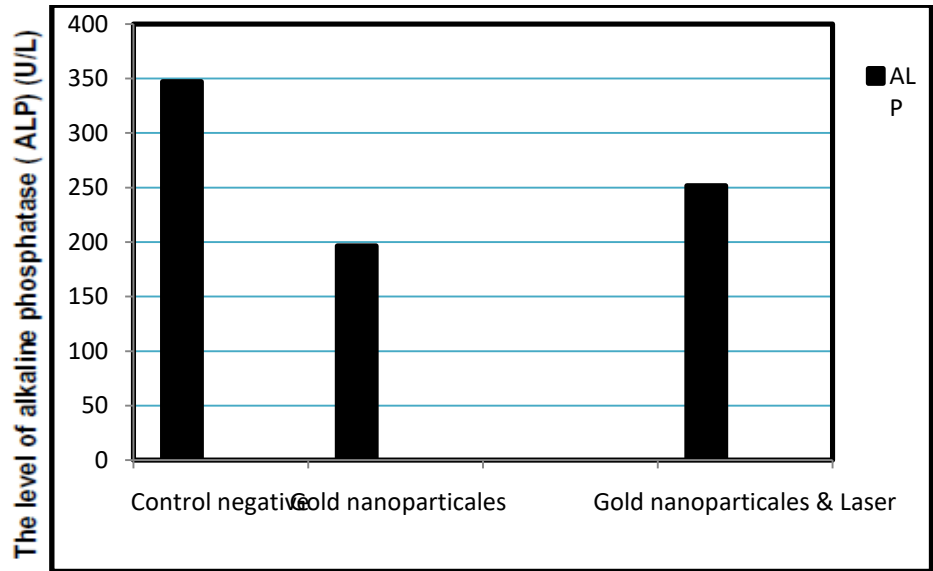


Figure 7: The levels of alkaline phosphatase (ALP) in different groups’ blood serum.

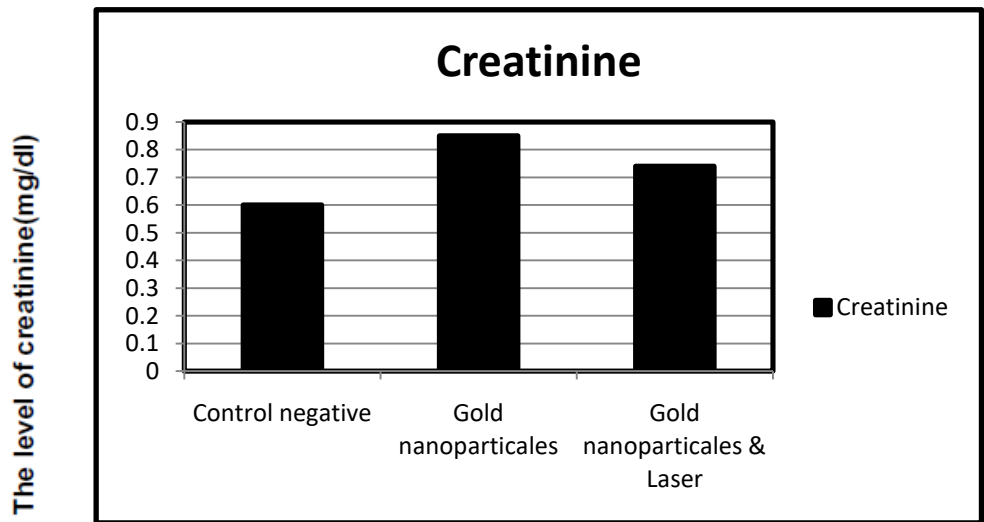


Figure 8: The levels of creatinine (CREA) in different groups’ blood serum.

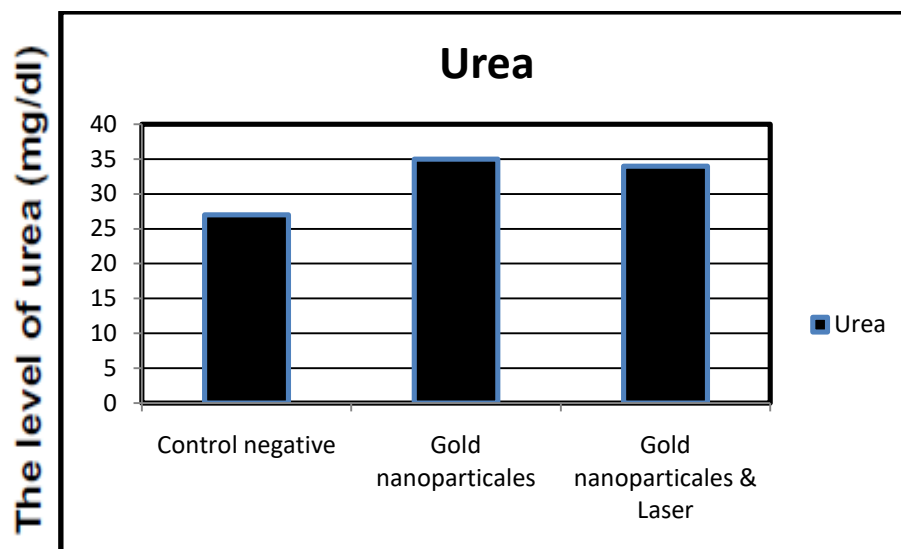


Figure 9: The levels of urea (UREA) in different groups' blood serum.

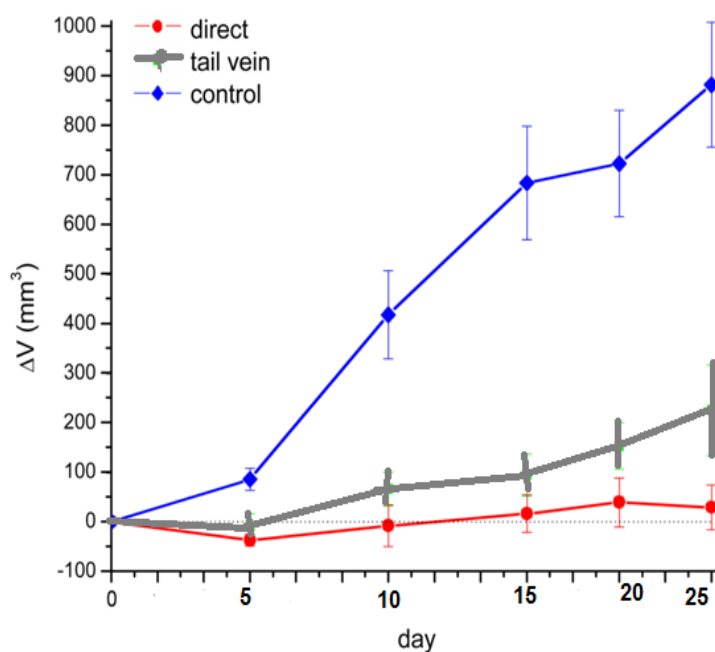





Figure10 Average change in tumor volume for SCC following near-infrared PPTT treatment by control (, intravenous (, and direct () injection of pegylated goldnanospheres.while intravenous treatments were performedby administration of 100 μ Lpegylated gold nanospheres. Direct PPTT treatments wereperformed by administration of 15 μ Lpegylated gold nanorods followed by 24 h of 0.9W/cm² NIR laser exposure.

Table 1: The levels of Aspartate transaminase (AST), gamma glutamyltransferase (GGT), Alanine transferase (ALT), alkaline phosphatase (ALP), creatinine (CREA) and urea (UREA) in different groups' blood serum.

	AST	GGT	ALT	ALP	Creatinine	Urea
Control negative	130	15	44	347	0.6	27
Gold nanoparticules	135	25	40.5	196.6	0.85	35
Gold nanoparticules & Laser	139	22	39	251.6	0.74	34

Table 2: P-values for average volume change in SCC tumors following near-infrared PPTT by 808 nm irradiation of pegylated gold nanospheres.

	day 0	day 5	day 10	day 15	day 20	Day 29
direct vs control	0	0.0003	0.001	0.0002	0.0001	0.0001
tail vein vs control	0	0.0136	0.0037	0.0005	0.0004	0.0008
direct vs tail	0	0.3415	0.1896	0.1936	0.1205	0.084

Table 3: Non-parametric analysis of variance for nearinfrared PPTT treatment (2) and control groups.

day 0	day 5	day 10	day 15	day 20	Day 29
0	0.0024	0.0009	0.0008	0.0001	0.0005